

Metal–Organic Frameworks with Exceptionally High Methane Uptake: Where and How is Methane Stored?

Hui Wu,^[a, b] Jason M. Simmons,^[a] Yun Liu,^[a, c] Craig M. Brown,^[a] Xi-Sen Wang,^[d] Shengqian Ma,^[d] Vanessa K. Peterson,^[e] Peter D. Southon,^[f] Cameron J. Kepert,^[f] Hong-Cai Zhou,^[d] Taner Yildirim,^[a, g] and Wei Zhou*^[a, b]

Abstract: Metal–organic frameworks (MOFs) are a novel family of physico-sorptive materials that have exhibited great promise for methane storage. So far, a detailed understanding of their methane adsorption mechanism is still scarce. Herein, we report a comprehensive mechanistic study of methane storage in three milestone MOF compounds (HKUST-1, PCN-11, and PCN-14) the CH₄ storage capacities of which are among the highest reported so far among all porous materials. The three MOFs consist of the same dicopper paddlewheel secondary building units, but contain different organic linkers, leading to cage-like pores with various sizes and geometries. From neutron

powder diffraction experiments and accurate data analysis, assisted by grand canonical Monte Carlo (GCMC) simulations and DFT calculations, we unambiguously revealed the exact locations of the stored methane molecules in these MOF materials. We found that methane uptake takes place primarily at two types of strong adsorption site: 1) the open Cu coordination sites, which exhibit enhanced Coulomb attraction toward methane, and 2) the

Keywords: adsorption • metal–organic frameworks • methane storage • neutron diffraction • physisorption

van der Waals potential pocket sites, in which the total dispersive interactions are enhanced due to the molecule being in contact with multiple “surfaces”. Interestingly, the enhanced van der Waals sites are present exclusively in small cages and at the windows to these cages, whereas large cages with relatively flat pore surfaces bind very little methane. Our results suggest that further, rational development of new MOF compounds for methane storage applications should focus on enriching open metal sites, increasing the volume percentage of accessible small cages and channels, and minimizing the fraction of large pores.

Introduction

Energy storage is a prime challenge facing chemists in the 21st century. Methane, the principle component of natural

gas, is an attractive fuel due to its natural abundance and clean burning process. To facilitate its use in automobiles, intense research efforts have been carried out to find suitable porous materials to store methane in a safe, cheap, and con-

[a] Dr. H. Wu, Dr. J. M. Simmons, Dr. Y. Liu, Dr. C. M. Brown, Prof. Dr. T. Yildirim, Dr. W. Zhou
NIST Center for Neutron Research, National Institute of Standards and Technology, Gaithersburg, Maryland 20899 (USA)
Fax: (+1)301-921-9847
E-mail: wzhou@nist.gov

[b] Dr. H. Wu, Dr. W. Zhou
Department of Materials Science and Engineering
University of Maryland, College Park, Maryland 20742 (USA)


[c] Dr. Y. Liu
Department of Chemical Engineering, University of Delaware
Newark, Delaware 19716 (USA)

[d] Dr. X.-S. Wang, Dr. S. Ma, Prof. H.-C. Zhou
Department of Chemistry, Texas A&M University
College Station, Texas 77842 (USA)

[e] Dr. V. K. Peterson
Bragg Institute, Australian Nuclear Science & Technology Organisation, NSW 2234 (Australia)

[f] Dr. P. D. Southon, Prof. C. J. Kepert
School of Chemistry, University of Sydney
NSW 2006 (Australia)

[g] Prof. Dr. T. Yildirim
Department of Materials Science and Engineering
University of Pennsylvania, Philadelphia, Pennsylvania 19104 (USA)

 Supporting information for this article is available on the WWW under <http://dx.doi.org/10.1002/chem.200902719>.

venient manner without the need for a massive pressure containment vessel. In 2000, the U.S. Department of Energy (DOE) set the target for material-based adsorbed methane storage at $180 \text{ cm}^3(\text{STP})\text{cm}^{-3}$ at 298 K and 35 bar, in which $\text{cm}^3(\text{STP})\text{cm}^{-3}$ means the standard temperature and pressure equivalent volume of methane per volume of the adsorbent material.^[1] This volumetric storage capacity target is comparable to methane compressed at 250 bar (298 K), in terms of energy density. Among various porous materials studied,^[2] traditional zeolites typically exhibit methane uptake below $100 \text{ cm}^3(\text{STP})\text{cm}^{-3}$, whereas most porous carbon materials show uptake in the range of approximately $50\text{--}160 \text{ cm}^3(\text{STP})\text{cm}^{-3}$. Some porous carbon materials have been reported to modestly meet the DOE target,^[3] yet the room to further improve their storage capacities is limited because of the difficulty in increasing their already high surface areas ($\approx 2000\text{--}3500 \text{ m}^2\text{g}$), which are known to strongly correlate to the methane adsorption capacities in these materials.^[2]

Metal–organic frameworks (MOFs) are a relatively new family of nanoporous materials that also offer great promise for methane storage.^[4] In general, MOFs possess many novel structural features (such as open metal coordination sites and versatile organic linkers) and gas adsorption properties not found in traditional porous materials. Several MOF compounds have been reported to exhibit exceptional methane uptake at room temperature and 35 bar,^[5–10] up to around $220 \text{ cm}^3(\text{STP})\text{cm}^{-3}$. Compared with porous carbon materials, an advantage of MOF materials is their ordered crystal structures, which make it possible to determine exactly where methane molecules are adsorbed and stored, and enable further understanding of the methane binding mechanism at these sites. Clearly, such information would provide key guidance for further, rational development of new MOF materials tailored towards improved methane storage. Considering the vast number of metal clusters and organic linkers available for the synthesis of new MOF compounds, the potential to achieve appreciably higher methane storage capacities is significant.

Recently, we have reported the primary methane adsorption sites in two classical MOF compounds, MOF-5 [$\text{Zn}_4\text{O}(\text{bdc})_3$] ($\text{bdc}=1,4\text{-benzenedicarboxylate}$) and ZIF-8 [$\text{Zn}(\text{MeIM})_2$] ($\text{MeIM}=2\text{-methylimidazolate}$), in which the methane interaction with the framework is of typical van der Waals (vdW) type.^[11] We have also reported the methane adsorption sites in a series of $\text{M}_2(\text{dhtp})$ MOFs ($\text{M}=\text{open metal}$, $\text{dhtp}=2,5\text{-dihydroxyterephthalate}$; also known as MOF-74 analogues), in which methane adsorption occurs primarily on the coordinatively unsaturated metal ions through enhanced Coulomb interaction.^[12] These two examples represent special cases where only one type of interaction is dominant. The situation is more complicated in most other MOF materials that exhibit interesting methane adsorption behavior; several types of interaction are likely to coexist and all contribute to the total methane storage capacities. Related to the binding mechanism is the important unanswered question, that is, which structural characteristic

is the most crucial to high capacity methane uptake in MOFs: pore size, pore geometry, surface area, or something else?

Herein, we address this question by elucidating the primary methane adsorption mechanisms through the determination of binding sites in three important MOF compounds (see Figure 1): HKUST-1 [$\text{Cu}_3(\text{btc})_2$] ($\text{btc}=1,3,5\text{-benzenetricarboxylate}$), PCN-11 [$\text{Cu}_2(\text{sbtc})$] ($\text{sbtc}=\textit{trans}\text{-stilbene-3,3',5,5'-tetracarboxylate}$), and PCN-14 [$\text{Cu}_2(\text{adip})$] ($\text{adip}=5,5'-(9,10\text{-anthracenediyl})\text{diisophthalate}$). These MOF compounds all exhibit impressive excess methane adsorption capacities at room temperature and 35 bar: around 160, 170, and $220 \text{ cm}^3(\text{STP})\text{cm}^{-3}$, respectively.^[7–9] HKUST-1 is one of the most widely studied MOF compounds,^[13] whereas PCN-14 has the highest volumetric methane uptake among all porous materials reported so far.^[8] Structurally, all three compounds contain the same dinuclear $\text{Cu}_2(\text{CO}_2)_4$ “paddle-wheel” clusters, but different organic linkers, which lead to cage-like pores with different sizes and geometries (see Figure 1). The topological diversity of this series of compounds provides an excellent opportunity for us to evaluate the role of pore structure and linker functionality on methane adsorption.

As already revealed in our recent study on $[\text{M}_2(\text{dhtp})]$ MOFs, the open metal coordination sites exhibit relatively high affinity for methane molecules.^[12] Naturally, the open Cu sites in HKUST-1, PCN-11, and PCN-14 are expected to be a primary methane adsorption site. Direct binding of one methane molecule is possible at each Cu site, but only accounts for a small fraction of the total storage capacity as measured at room temperature and 35 bar in these MOFs. Hence, there must be a large number of other strong adsorption sites. To reveal these additional methane binding sites, we performed systematic neutron powder diffraction experiments on these MOFs loaded with various amounts of methane. From detailed diffraction data analysis and Rietveld structural refinements, assisted by grand canonical Monte Carlo (GCMC) simulations^[14] and DFT calculations, we were able to directly determine the methane locations and orientations in these MOFs with high accuracy. This information enables us for the first time to correlate the methane locations and adsorption energies with the MOF framework compositions and pore structures, gaining insights into the origin of the high-capacity methane uptake in these milestone MOF materials.

Results and Discussion

To facilitate our data presentation and discussion, we first briefly describe and compare the structural characteristics of the three MOFs (see Figure 1). Each MOF structure contains two to three types of cage-like pore, which are interconnected at “windows”. Because of their different organic linkers, the pore size and/or topology are different in the three structures. HKUST-1 has the highest symmetry ($Fm\bar{3}m$) of the three, due to the high symmetry of the btc

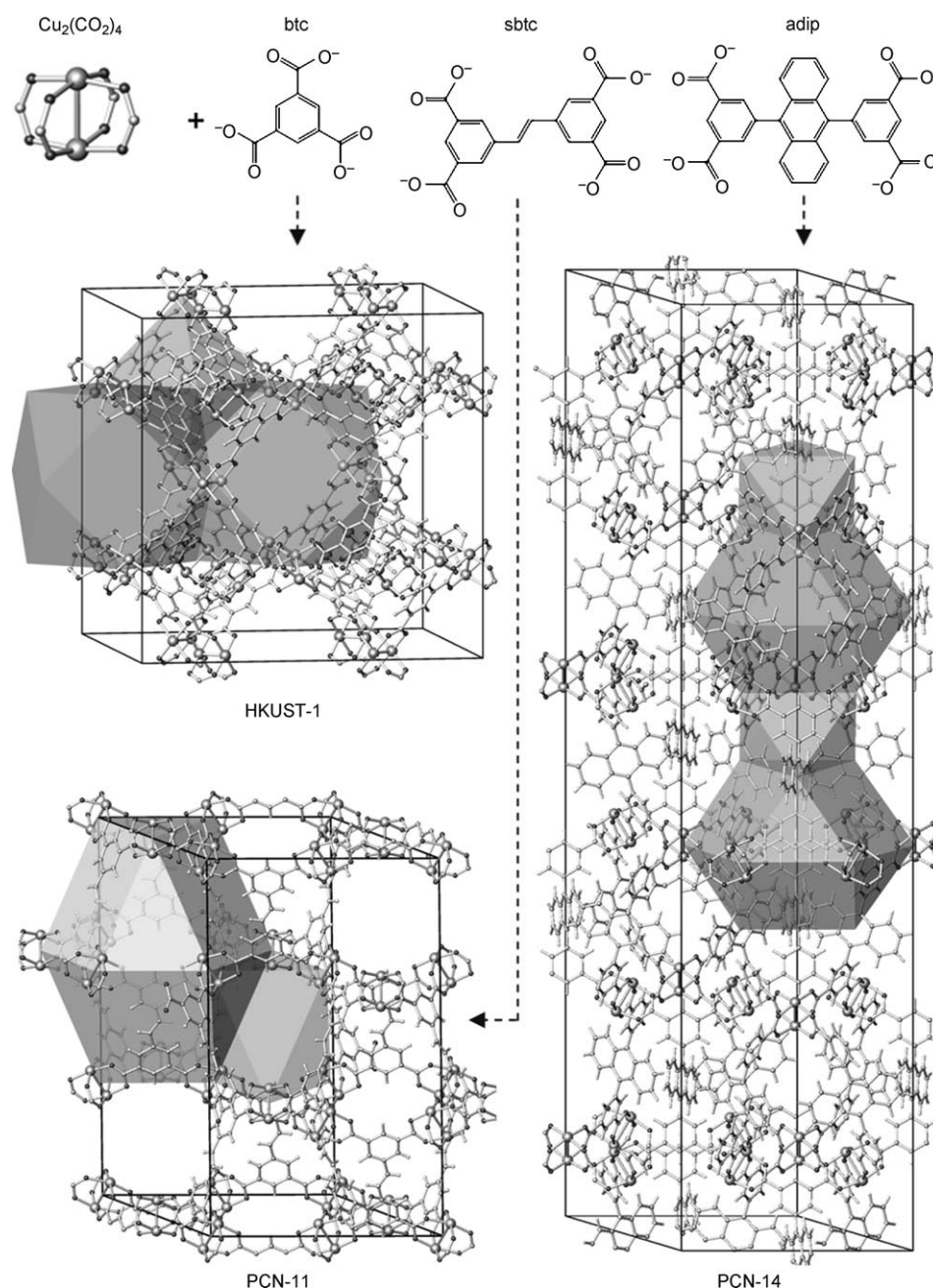


Figure 1. Crystal structures of HKUST-1, PCN-11, and PCN-14. Note that the three MOFs consist of the same $\text{Cu}_2(\text{CO}_2)_4$ secondary building units, but different organic linkers. The Cu ions are coordinatively unsaturated (with a coordination number of five), unlike the vast majority of Cu-containing MOFs, including those that contain the paddlewheel, but in which it bridges through the apical Cu site and consequently the Cu site is fully coordinated and saturated. The polyhedral cages in the Figure represent the pore structures in these MOF compounds (see text for detailed description).

linker. Importantly, it can also be described by using a lower symmetry of $R\bar{3}$ (the crystal symmetry of PCN-11) with a larger unit cell and more “independent” atoms. This lowered symmetry is essential to properly describe the HKUST-1 structure adsorbed with methane molecules (the structural model with $Fm\bar{3}m$ symmetry and orientationally disordered methane was found to fit poorly to the experimental diffrac-

tion data). The small pore (in the octahedral cage) in HKUST-1 has a dimension of approximately 4 Å whereas the two large pores (in the cuboctahedral cages I and II) are around 10 and 11 Å, respectively. In PCN-11, the size of the small pore (in the octahedral cage) is around 7 Å, whereas the large pore (in the elongated cuboctahedral cage) has dimensions of approximately 10 and 16 Å in the two distinctive directions. The network architecture of PCN-14 (with crystal symmetry $R\bar{3}c$) is somewhat similar to PCN-11. The primary difference is that the cuboctahedral cage of PCN-11 is broken into three cages in PCN-14 by the anthracenyl rings: one squashed cuboctahedral cage at the center and two small cages on the top and bottom. This small cage has an approximately 3 Å accessible internal void. The dimensions of the two large pores (in the cuboctahedral cages I and II) are about 11×11 and 11×4 Å, respectively. Interestingly, in the three structures, the exposed “surfaces” of the coordinatively unsaturated Cu ions are all present in one single cage: the cuboctahedral cage I in HKUST-1 and PCN-14, and the octahedral cage in PCN-11. The internal surfaces of these cages would be fully coated if each open Cu ion adsorbed one CH_4 molecule.

The neutron powder diffraction data that we collected on the MOF samples loaded with various amounts of methane, in principle, contain all the structural information that we are looking for (in particular, the location and orientation of the adsorbed methane). In reality, directly solving the adsorbate structure from a diffraction pattern is only possible for simple systems. When analyzing the diffraction data from a MOF material with adsorbed guest molecules, the Fourier difference technique is usually very helpful for solving the structure of the guest molecules.^[14,15] Application of this method requires that the sym-

metry of the crystal remains unchanged upon the addition of guest molecules. Unfortunately, in MOFs with high symmetry (e.g., HKUST-1), the CH₄ molecule symmetry is not always compatible with the MOF site symmetry. For MOFs with relatively large unit cells (e.g., PCN-11 and PCN-14), the large number of independent atoms (variables) induces additional difficulties to the data analysis.

To tackle this problem and facilitate the diffraction data analysis, we employed GCMC simulations^[16] of methane adsorption in these MOF structures by using the classical force-field method, which gave clues regarding the possible major methane molecule adsorption sites, in addition to the expected open Cu sites. Simulations were performed on the three MOFs at 298 K and various pressures (0.1, 1, 10, and 35 bar). The probability distribution of adsorbed CH₄ was generated from the simulation after the equilibrium stage, which clearly revealed several locations that are highly populated by CH₄ molecules. Figure 2 shows the simulation results obtained at a pressure of 10 bar as an example. As explained in the method section, the open Cu sites are underpopulated with methane because of the intrinsic limitation of classical force fields in describing enhanced interactions; however, we know that the open Cu sites must be one of the primary sites, based on our previous work.

As shown in Figure 2 (top-left panel), the four window openings of the small octahedral cage in HKUST-1 are clearly rich in adsorbed methane, and we term this the “small cage window site”. There is also some methane population at the center of the small octahedral cage and at the corner of the large cuboctahedral cage II. We call these two sites the “small cage center site” and “large cage corner site”, respectively.

Similar to HKUST-1, in PCN-11, there is significant methane population at the cage window site (Figure 2, bottom-left panel). At low pressure (0.1 bar), only one methane rich area is revealed near the center of the window, similar to that observed for HKUST-1. With increasing pressure, methane molecules begin populating both sides of the window opening, leading to two distinctive cage window sites (termed I and II). In addition to the open

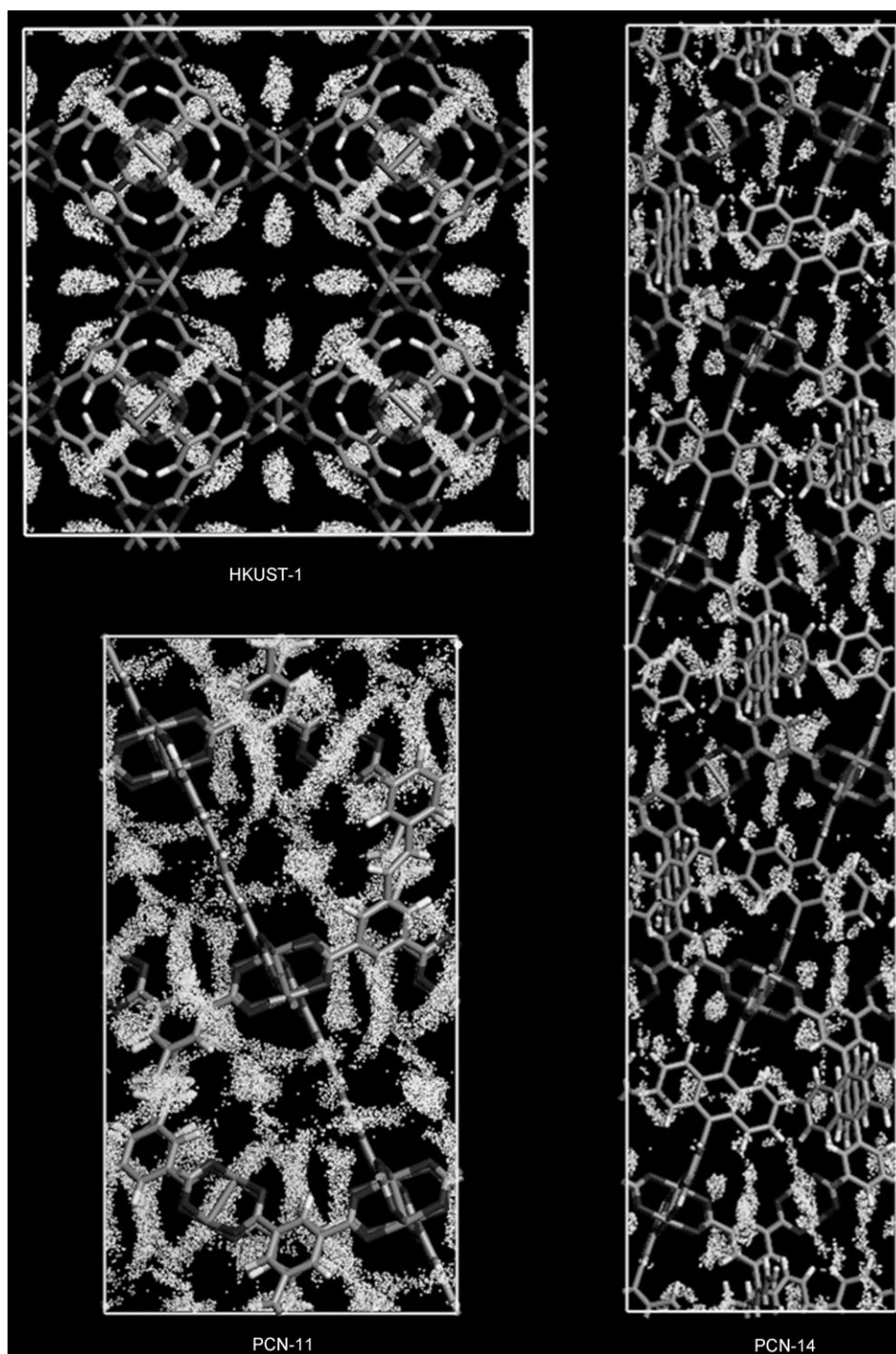


Figure 2. Probability distribution of the CH₄ center of mass in HKUST-1, PCN-11, and PCN-14 ([0 1 0] view), obtained from GCMC simulations at 298 K and 10 bar.

Cu site and the cage window sites, two additional methane adsorption sites within the large elongated cuboctahedral cage, are also apparent, although they are less populated and their locations are not as well defined compared with the cage window sites. We term these minor sites “large cage corner site I” and “large cage corner site II”.

In PCN-14, a significant methane population also exists at the cage window sites (Figure 2, right panel). However, due to the extra small cage derived from the anthracenyl rings, one of the analogous cage window sites (cage window site II in PCN-11) is actually located within the small cage towards the bottom, thus termed “small cage bottom site”. This small cage also has three narrow side windows (with a window opening size of only about 1 Å) that are populated with a considerable amount of methane on the outside of the window and are termed “small cage side window sites”. Minor methane population was found at the corners of the large cuboctahedral cage II, which were termed “large cage corner site I” and “large cage corner site II”, respectively.

These preferred methane binding sites in the three MOFs provide important, qualitative clues for analyzing the experimental diffraction data, as Rietveld refinement on the diffraction data requires a structure model reasonably close to the “real structure” of the targeted system. Guided by the methane locations derived from our GCMC simulations, such a structural model is readily available and the difficulty of analyzing the experimental diffraction data is greatly reduced. We were able to perform full-profile Rietveld refinements by using the neutron powder diffraction data of HKUST-1 and PCN-11 containing various amounts of methane, and thus to directly determine the methane locations and orientations in the two MOFs with high accuracy. (The data of PCN-14 are not included here because its large unit cell makes the structural refinement formidable.) As noted above, we use the lower symmetry $R\bar{3}$ space group to describe HKUST-1 because the symmetry of the adsorbed methane is incompatible with the $Fm\bar{3}m$ symmetry of the bare HKUST-1 lattice. Representative refinement plots are shown in Figure 3. The refined CD_4 coordinates along with the detailed information of the host crystal structure and diffraction patterns at low methane loading are provided in the Supporting Information (see Tables S1–S3 and Figure S1). Interestingly, the locations and relative populations of the adsorbed methane at all the major binding sites (except the open Cu sites) derived experimentally from the Rietveld refinement agree well with those predicted by GCMC simulations. For example, in HKUST-1, for the 1.1 CD_4/Cu loading, the open Cu site and the small cage window site are heavily populated with similar occupancies, whereas the small cage center site and large cage corner site are only slightly populated. In PCN-11, a large methane loading of 2.8 CD_4/Cu clearly shows that the two primary adsorption sites (the open Cu site and the cage window site I) are fully occupied, whereas the cage window site II and the two large cage corner sites are partially populated. The qualitative agreement between the experimental results and the GCMC simulation suggests that the classical force

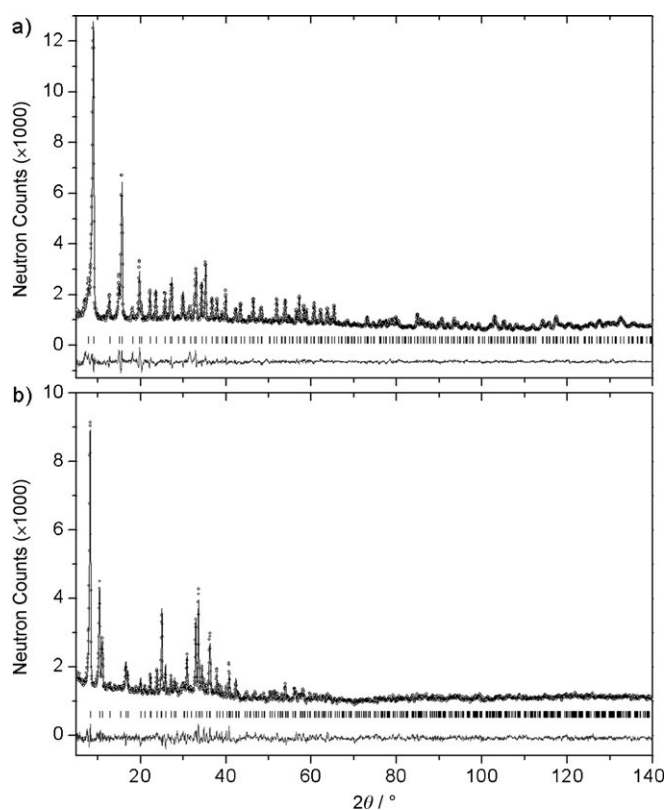


Figure 3. Observed (dots), refined (line), and difference (noisy line) neutron powder diffraction profiles for a) HKUST-1 with a CD_4 loading of 1.1 CD_4/Cu , and b) PCN-11 with a CD_4 loading of 2.8 CD_4/Cu . Further details: a) Space group = $R\bar{3}$, $a = 18.595(1)$ Å, $c = 45.536(6)$ Å; CD_4 site occupancies: open Cu site: 0.67(1), small cage window site: 0.59(1), small cage center site: 0.13(1), large cage corner site: 0.06(1); goodness of fit data: $R_{wp} = 0.0334$, $R_p = 0.0284$, $\chi^2 = 1.096$. b) Space group: $R\bar{3}$, $a = 18.564(1)$ Å, $c = 32.103(4)$ Å; CD_4 site occupancies: open Cu site = 1.0, cage window site II: 0.87(1), large cage corner site I: 0.76(1), large cage corner site II: 0.41(1); goodness of fit data: $R_{wp} = 0.0405$, $R_p = 0.0339$, $\chi^2 = 1.913$.

field that we used is able to capture the major vdW-type interaction between methane and the MOF framework.

The experimental structures of adsorbed methane can be further testified by DFT calculations. For HKUST-1 and PCN-11, we found that the DFT-optimized locations and orientations of the adsorbed methane molecules are in full agreement with the experimental results (see Tables S1–S3 and the CIF files in the Supporting Information). This observation extends confidence to our computational results on PCN-14, for which the experimental structural information of adsorbed methane is not available.

In Figures 4 to 6, we show in detail the positions and orientations of the adsorbed CH_4 at various adsorption sites in the three MOFs. Due to the large cell dimensions, partial structures are shown in the figures for clarity (for full crystal structures, see Figure S2 and the CIF files in the Supporting Information).

The methane binding configuration at the open Cu site is essentially the same in all three MOFs. As illustrated in Figure 4a for HKUST-1, the methane molecule assumes an ori-

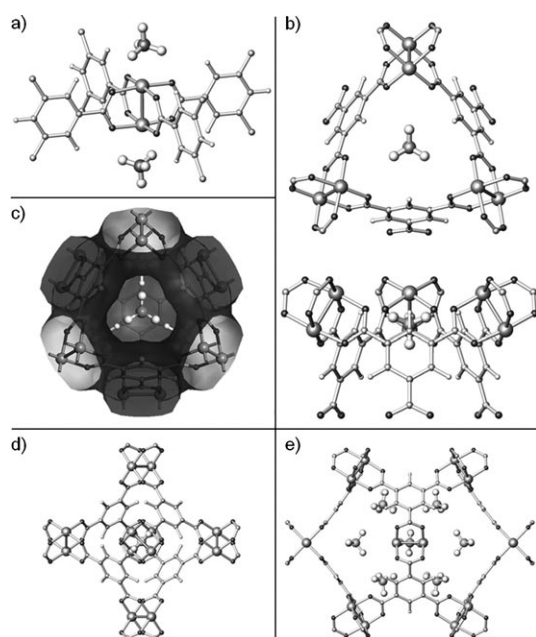


Figure 4. Experimentally determined partial structure of the HKUST-1 crystal with CH₄ molecules adsorbed at a) the open Cu sites and b) the small cage window sites (top and side views). c) vdW surface of the small octahedral cage in HKUST-1 (derived by using N₂ as probe molecules), showing the size and geometry of the pore window in an excellent match with a methane molecule. d) CH₄ molecule adsorbed at the center of the small octahedral cage, a secondary adsorption site. e) CH₄ molecule located at the large cage corner site, also a weak adsorption site.

entation such that it sits directly on top of the open Cu ion, similar to what we found previously for CH₄ binding in MOFs with other types of open metal centers.^[12] Figure 4b shows the adsorbed CH₄ at the small cage window site, in which one hydrogen atom of the relaxed methane molecule points toward the center of the small octahedral cage, and other three hydrogen atoms point to the surrounding Cu₂(CO₂)₄ units. Figure 4d and e correspond to adsorbed methane at the small cage center site and the large cage corner site (in the cuboctahedral cage II), both of which are secondary adsorption sites.

Figure 5a shows the methane geometry at the two cage window sites in PCN-11. Both CH₄ molecules are well aligned on the threefold axis of the large elongated cuboctahedral cage, with one hydrogen atom pointing to the cage center. Similar to the methane at the small cage window site in HKUST-1, the other three hydrogen atoms of the methane adsorbed in PCN-11 at the cage window site I point towards the Cu₂(CO₂)₄ units. In contrast, the other three hydrogen atoms of the methane at the cage window site II point to the organic linkers, reflecting the difference in its local potential surface compared with that of the cage window site I. Figure 5b shows the large cage corner site I, in which the methane location is fairly close to adjacent methane molecules at the open Cu site and cage window site II, and thus it is likely that at this site the methane interacts with both the pore surface of the elongated cuboctahedral cage and the surrounding methane molecules. These

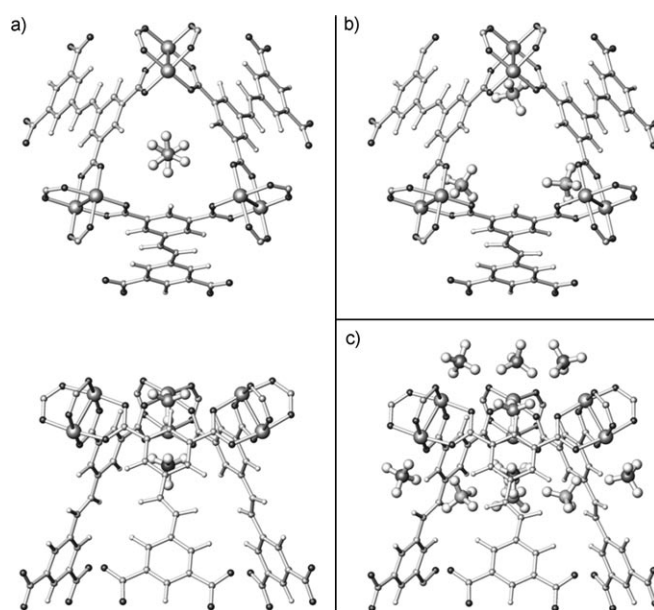


Figure 5. Experimentally determined partial structure of the PCN-11 crystal with CH₄ molecules adsorbed at a) the two cage window sites (top and side views), b) the large cage corner site I, and c) all four major adsorption sites, including the open Cu sites.

sites, along with the open Cu sites, provide the major adsorption sites for methane in PCN-11 and are shown in Figure 5c.

Similar structural information of adsorbed methane is shown for PCN-14 in Figure 6. Note that these are purely computational results, unlike in the cases of HKUST-1 and PCN-11. The DFT-relaxed small cage window site and small cage bottom site (Figure 6a) have great similarity to the two cage window sites presented in PCN-11 (Figure 5a), in terms of CH₄ location and orientation. Figure 6b shows the small cage side window site, a unique adsorption site not present in the other two MOFs. Figure 6c is the overall picture of the methane adsorbed at all four major sites in PCN-14. For completeness, in the Supporting Information, we also provided the methane structures at the two minor adsorption sites (cage corner sites I and II) in PCN-11 and PCN-14 (see Figure S2).

Thus far, we have addressed the structures of the major CH₄ adsorption sites in the three MOFs. Now we focus on the energy aspect of the adsorption. In Table 1, we summarize the DFT-calculated static methane binding energies on both the primary and secondary adsorption sites, along with the experimental, initial isosteric heats of adsorption (Q_{st}) from the literature. As expected, the local-density approximation (LDA) overestimates the methane binding strength, resulting in larger adsorption enthalpies than the experimental values. Also note that due to the intrinsic limitation of DFT on modeling physisorption, the values obtained represent only qualitative information. (Computation at a higher level than standard DFT is usually too costly and impractical on MOFs with large unit cells.) Nevertheless, the relative binding strength of methane at different adsorption sites

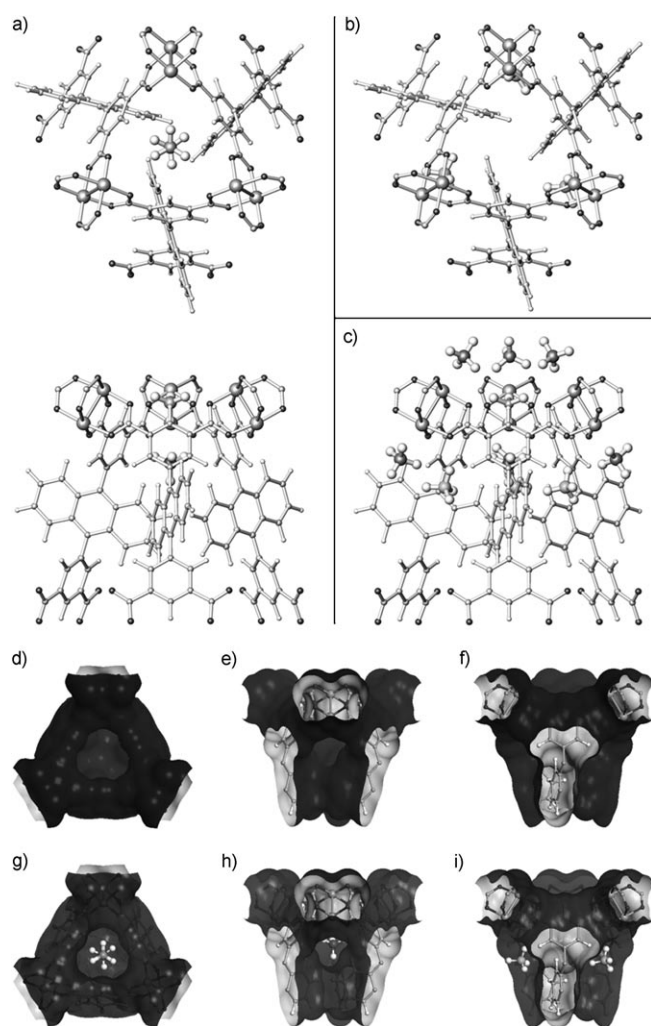


Figure 6. Partial structure of the DFT-optimized PCN-14 crystal with CH_4 molecules adsorbed at a) the small cage window site and the small cage bottom site (top and side views), b) the small cage side window site, and c) all four major adsorption sites, including the open Cu sites. d)–f) the vdW surface of the small cage in PCN-14 (top and side views). g)–i) the vdW surface with adsorbed methane. Note that the local potential surfaces of the small cage window site and the small cage bottom site are in perfect match with the adsorbed methane molecules, leading to enhanced vdW interaction.

found in our calculations follows the experimental trend (the site populations revealed from the diffraction data) reasonably well. The CH_4 binding energies at the open Cu sites are roughly identical in all three MOFs, that is, about 25 kJ mol^{-1} . The cage window sites have a similar CH_4 affinity, also around 25 kJ mol^{-1} . The small cage bottom site in PCN-14 has the highest calculated E_B of approximately 32 kJ mol^{-1} suggesting that this site is likely to be responsible for the exceptional initial Q_{st} measured in PCN-14. To put these values into perspective, the calculated CH_4 binding energy at the strongest binding site (the “cup site”) in MOF-5 is 20.7 kJ mol^{-1} ,^[12,17] whereas on a graphene surface it is approximately 17 kJ mol^{-1} (both calculated by us using similar methodologies). Clearly, the methane binding on the primary sites in the three MOFs studied here are all stron-

Table 1. Summary of data obtained for HKUST-1, PCN-11, and PCN-14.

MOF	exp CH_4 ads ^[a,e]		exp initial Q_{st} ^[b]		Primary adsorption sites		Secondary adsorption sites			
	$[\text{cm}^3(\text{STP})\text{cm}^{-3}]$	$[\text{cm}^3(\text{STP})\text{cm}^{-3}]$	$[\text{kJ mol}^{-1}]$	$[\text{kJ mol}^{-1}]$	site name	max CH_4 ads ^[c,e] $[\text{cm}^3(\text{STP})\text{cm}^{-3}]$	E_B ^[d] $[\text{kJ mol}^{-1}]$	site name	max CH_4 ads ^[c,e] $[\text{cm}^3(\text{STP})\text{cm}^{-3}]$	E_B ^[d] $[\text{kJ mol}^{-1}]$
HKUST-1	160 (1.65)	18.2	14.6	30.0	open Cu site	97 (1)	25.5	small cage center site	16 (1/6)	18.1
					small cage window site	65 (2/3)	24.8	large cage corner site	48 (1/2)	17.9
PCN-11	170 (2.43)	14.6	30.0	30.0	open Cu site	70 (1)	24.7	large cage corner site I	70 (1)	19.5
					cage window site I	23 (1/3)	25.0	large cage corner site II	70 (1)	15.7
PCN-14	220 (3.73)	18.2	14.6	30.0	cage window site II	23 (1/3)	22.0	large cage corner site I	59 (1)	18.9
					open Cu site	59 (1)	25.0	large cage corner site II	59 (1)	16.5
					small cage bottom site	20 (1/3)	32.0			
					small cage window site	20 (1/3)	25.8			
					small cage side window site	59 (1)	21.0			

[a] The experimental excess CH_4 adsorption capacity at RT and 35 bar (exp CH_4 ads). [b] The experimental initial isosteric heat of adsorption (Q_{st}) for CH_4 . [c] The saturated CH_4 adsorption capacity on each adsorption site (max CH_4 ads). [d] The calculated static binding energy of CH_4 on each adsorption (E_B , from DFT–LDA). [e] Values shown in parentheses are equivalent capacity in terms of “number of CH_4 molecules per Cu ion”. Note that the Q_{st} for HKUST-1 was not available from the literature, and thus was measured in this work (see the Supporting Information for details), whereas other experimental data for HKUST-1, PCN-11, and PCN-14 are from refs. [7], [9], and [8], respectively.

ger than typical vdW adsorption. For the open Cu sites, the binding enhancement is expected, since there is an improved Coulomb attraction between the exposed metal ion and the slightly polarized CH₄ molecule, as shown previously.^[12] Of particular interest is the enhanced methane binding at the cage window sites present in each MOF and the small cage bottom site in PCN-14, the magnitude of which is equal to or greater than that found on the open Cu site, despite the fact that the interaction is solely of vdW type. To explore the origin of this enhanced vdW interaction, in Figure 4c, we plot the vdW surface of the small octahedral cage in HKUST-1, derived by using N₂ as probe molecules. It is immediately evident that the cage window has a dimension and threefold symmetry that is well matched with an adsorbed methane molecule, leading to multiple interactions between the gas molecule and the surrounding framework. Similarly, in Figure 6d–i, we plot the vdW surface of the small cage of PCN-14, both with and without adsorbed methane. The top window of the cage has a geometry similar to that shown in Figure 4c for HKUST-1. The bottom of the cage is a deep potential pocket (Figure 6e and h), perfectly matching the tetrahedral molecular geometry of a methane molecule locked inside the cage, resulting in a greatly enhanced vdW interaction. The side windows, although not perfectly shaped to accommodate interaction with a methane molecule, also generate a somewhat enhanced vdW interaction toward methane. Clearly, the enhanced vdW interaction originating from potential pockets plays an important role in generating some of the strong CH₄ adsorption sites found in these MOF compounds.

Next, we discuss how these major adsorption sites, listed in Table 1, account for the high capacity methane uptake found under technologically relevant conditions. For HKUST-1, full saturation of the primary sites yields a methane capacity of around 160 cm³(STP)cm⁻³, roughly equal to the experimental uptake measured at 298 K and 35 bar. In reality, some secondary sites begin to populate before the primary sites are fully populated (as is evident in the diffraction data; presumably following the Maxwell–Boltzmann distribution), although their contribution to the total methane uptake is minor. Similarly, in PCN-11, full saturation of the primary sites can generate a methane capacity of about 120 cm³(STP)cm⁻³, which is approximately 70% of the experimental uptake at 298 K and 35 bar. Partial population of the secondary large cage corner sites can well account for the difference. In PCN-14, the small cage window sites, small cage bottom sites, open Cu sites, and small cage side window sites altogether would give around 160 cm³(STP)cm⁻³ storage capacity, which is approximately 75% of the total uptake. As in PCN-11, the secondary large cage corner sites can easily provide the remaining storage capacity.

From our analyses, some similarity between MOFs and other porous media used for methane storage can be identified. In terms of pore size and geometry, accessible, smaller pores (i.e., pores with dimensions comparable or slightly larger than the kinetic diameter of methane (≈3.8 Å)) are

preferred in all porous storage materials, providing improved vdW interaction with methane compared with large pores. There are also unique features associated with MOF materials. In traditional porous carbon materials or polymeric materials, the methane binding on the pore surface is generally weak and uniform, and thus methane uptake strongly correlates with the pore surface area.^[2] Improving the specific pore surface area and pore volume is the major route to improve their methane storage capacity. The same is also true for classical MOFs with only weak vdW adsorption sites, as found previously.^[6] In contrast, MOFs with high methane storage capacities, such as those studied in this work, contain various strong adsorption sites built into their pore surface. These sites dominate the methane uptake and diminish the role played by weak surface binding sites, making the pore surface area a less important factor. Of course, high surface area and pore volume are still necessary to accommodate enough methane molecules, but the surface area is less strongly correlated with the methane uptake at room temperature and 35 bar. This is clearly shown in Table 2 for several MOF compounds. For example, PCN-14 has an experimental Brunauer–Emmett–Teller (BET) surface area lower than MOF-5, but its methane storage capacity is twice that of the latter.

Table 2. Experimental N₂ Brunauer–Emmett–Teller surface areas and excess methane adsorption capacity (RT, 35 bar) of several MOF compounds from the literature.^[a]

MOF	exp N ₂ BET surface area [m ² cm ⁻³]	exp CH ₄ ads [cm ³ (STP)cm ⁻³]	Reference
MOF-5	1870	110	[17]
HKUST-1	1511	160	[13, 7]
PCN-11	1446	170	[9]
PCN-14	1453	220	[8]
Ni ₂ (dhtp)	1240	190	[12]

[a] Note that the BET surface areas reported in the literature are typically in the units of m²g⁻¹. Here we adopt the unit of m²cm⁻³ to properly correlate the pore surfaces areas with methane adsorption capacities reported on a volume basis. The surface area values were converted from m²g⁻¹ to m²cm⁻³ by multiplying by the crystal density (gcm⁻³).

Finally, we evaluate the importance of the linker functionality for methane adsorption. In particular, we are interested in the role of aromatic rings, since previous work has implied that the presence of aromatic rings on the organic linker can enhance CH₄ adsorption.^[6,8] Surprisingly, in all three MOF compounds investigated, none of the major adsorption sites is directly on top of the aromatic rings, although the surface of the organic linkers is still largely available after the primary sites have been occupied. This implies that the ability of the aromatic ring to attract a CH₄ molecule might not be as strong as was previously believed. To further confirm this, we directly calculated the methane binding strength on top of the aromatic ring in these MOFs and found that it is slightly weaker than methane adsorption on a graphene layer (≈15 vs. 17 kJmol⁻¹). Therefore, the methane interaction with an isolated aromatic ring is of typi-

cal weak vdW type. Although the specific CH₄–benzene interaction may be small, the addition of aromatic rings can lead to the formation of small cages or areas of significant potential overlap with enhanced vdW interactions. It is this secondary effect of the additional phenyl rings that leads to the impressive CH₄ uptake in PCN-14.

Conclusion

By determining the major methane adsorption sites in three important MOF compounds that exhibit great methane storage capacities, we found the structural features that are responsible for their high methane uptake. Methane adsorption takes place through two major binding mechanisms: 1) enhanced Coulomb interaction with the coordinatively unsaturated metals, and 2) enhanced vdW interaction at potential pocket sites. Our results suggest that open metal sites and accessible small cages/channels are favorable structural features for methane storage. Surface area and linker functionality are less important parameters to consider when developing new MOFs for methane storage applications. These findings may also have some general implications on the storage of other gas molecules, since the two major binding mechanisms described here also widely exist in many other gas–MOF systems.

Experimental Section

HKUST-1 and PCN-11 samples used in our diffraction experiment are the same as those used in previous work, in which the sample synthesis and activation processes were described in detail.^[15,9] Neutron powder diffraction measurements were performed on the bare MOFs and the same samples loaded with various amounts of CD₄ (see the Supporting Information for more technical details). Deuterated methane was used for the purpose of obtaining higher quality diffraction spectra, by avoiding the large incoherent neutron scattering cross section of hydrogen present in CH₄. CD₄ gas was loaded into the sample at RT and then slowly cooled to 4 K before the measurement was taken. Data were collected by using the high resolution neutron powder diffractometer (BT-1) at the NIST Center for Neutron Research. Rietveld structural refinements were performed by using the GSAS package.^[18]

GCMC simulations^[16,19] were performed for CH₄ adsorption in the three MOF compounds, with both the CH₄ molecules and the frameworks treated as rigid bodies. Appropriate MOF supercells were chosen as the simulation boxes so that the dimensions were larger than 30 × 30 × 30 Å³ to ensure simulation accuracy. 2 × 10⁷ steps were used for equilibration and an additional 2 × 10⁷ steps were used to calculate the ensemble average of CH₄ adsorption sites and thermodynamic properties. Since our goal in this work was to obtain the qualitative probability distributions of adsorbed CH₄, rather than the quantitative adsorption isotherms, we chose the standard universal force field (UFF) to describe the methane–framework interaction and the methane–methane interaction. It is important to note that the UFF does not accurately predict adsorption on the open metal sites, as most of the widely used empirical force fields cannot properly capture enhanced interactions. Nonetheless, this limitation does not affect the qualitative determination of the other framework sites, since the major vdW-type interaction between methane and the framework can be relatively well described by the UFF. Atomic partial charges derived from first-principles calculations (see Table S4 in the Supporting Information) were included in the simulation to account for electrostatic

interactions. More technical details of our GCMC simulations are provided in the Supporting Information.

First-principles calculations based on DFT were performed by using the plane-wave self-consistent field (PWSCF) package.^[20] Vanderbilt-type ultrasoft pseudopotentials and the LDA with the Perdew–Zunger exchange correlation were used. Generalized gradient approximation was not considered here, because it severely underestimates the binding, particularly between the open metal site and the methane molecule, as found in our previous study.^[12] A cutoff energy of 544 eV and a *gamma*-point *k* sampling were sufficient for the total energy to converge within 0.5 meVatom⁻¹. We first optimized the primitive cells of the MOF structures. CH₄ molecules were then introduced to the optimized MOF structures (guided by the GCMC results), followed by a full structural relaxation. To obtain the CH₄ binding energies, a CH₄ molecule placed in a supercell with the same cell dimensions was also relaxed as a reference. The static binding energy was then calculated by using Equation (1):

$$E_B = \frac{[E(\text{MOF}) + nE(\text{CH}_4) - E(\text{MOF} + n\text{CH}_4)]}{n} \quad (1)$$

Acknowledgements

This work was partially supported by the U.S. Department of Energy through BES grant no.: DE-FG02-08ER46522 (T.Y.). J.M.S. acknowledges support from the National Research Council Postdoctoral Associate Program. The work at Texas A&M University was partially supported by the U.S. Department of Energy (DE-FC36-07GO17033) and the National Science Foundation (CHE-0449634).

- [1] T. Burchell, M. Rogers, *SAE Tech. Pap. Ser.* **2000**, 2001–2205.
- [2] a) V. C. Menon, S. J. Komarneni, *J. Porous Mater.* **1998**, *5*, 43–58; b) D. Lozano-Castelló, J. Alcaniz-Monge, M. A. Casa-Lillo, D. Cazorla-Amoros, A. Linares-Solano, *Fuel* **2002**, *81*, 1777–1803.
- [3] P. Pfeifer, J. W. Burress, M. B. Wood, C. M. Lapilli, S. A. Barker, J. S. Pobst, R. J. Cepel, C. Wexler, P. S. Shah, M. J. Gordon, G. J. Suppes, S. P. Buckley, D. J. Radke, J. Ilavsky, A. C. Dillon, P. A. Parilla, M. Benham, M. W. Roth, *Mater. Res. Soc. Symp. Proc.* **2008**, *1041*, 1041-R02–02.
- [4] a) G. Férey, *Chem. Soc. Rev.* **2008**, *37*, 191–214; b) R. E. Morris, P. S. Wheatley, *Angew. Chem.* **2008**, *120*, 5044–5059; *Angew. Chem. Int. Ed.* **2008**, *47*, 4966–4981.
- [5] a) S.-i. Noro, S. Kitagawa, M. Kondo, K. Seki, *Angew. Chem.* **2000**, *112*, 2161–2164; *Angew. Chem. Int. Ed.* **2000**, *39*, 2081–2084; b) M. Kondo, M. Shimamura, S.-i. Noro, S. Minakoshi, A. Asami, K. Seki, S. Kitagawa, *Chem. Mater.* **2000**, *12*, 1288–1299; c) M. Eddaoudi, J. Kim, N. Rosi, D. Vodak, J. Wachter, M. O’Keeffe, O. M. Yaghi, *Science* **2002**, *295*, 469–472; d) S. Bourrelly, P. L. Llewellyn, C. Serre, F. Millange, T. Loiseau, G. Férey, *J. Am. Chem. Soc.* **2005**, *127*, 13519–13521.
- [6] T. Düren, L. Sarkisov, O. M. Yaghi, R. Q. Snurr, *Langmuir* **2004**, *20*, 2683–2689.
- [7] I. Senkovska, S. Kaskel, *Microporous Mesoporous Mater.* **2008**, *112*, 108–115.
- [8] S. Ma, D. Sun, J. M. Simmons, C. D. Collier, D. Yuan, H.-C. Zhou, *J. Am. Chem. Soc.* **2008**, *130*, 1012–1016.
- [9] X.-S. Wang, S. Ma, K. Rauch, J. M. Simmons, D. Yuan, X.-S. Wang, T. Yildirim, W. C. Cole, J. J. Lopez, A. De Meijere, H.-C. Zhou, *Chem. Mater.* **2008**, *20*, 3145–3152.
- [10] Note that the adsorption capacity directly obtained from experimental measurement is often gravimetric capacity (i.e., amount of adsorbed methane per unit mass of the MOF sample). The volumetric methane adsorption capacities in MOF materials reported in the literature are typically converted from the gravimetric values based on the ideal densities of MOF crystals. They thus represent the material performance of ideal, single crystal samples. In practice, there are still strong demands for discovering novel MOF materials with even

- higher ideal storage capacities than known MOFs to achieve the targeted storage capacity in terms of system performance.
- [11] H. Wu, W. Zhou, T. Yildirim, *J. Phys. Chem. C* **2009**, *113*, 3029–3035.
- [12] H. Wu, W. Zhou, T. Yildirim, *J. Am. Chem. Soc.* **2009**, *131*, 4995–5000.
- [13] S. S. Y. Chui, S. M. F. Lo, J. P. H. Charmant, A. G. Orpen, I. D. Williams, *Science* **1999**, *283*, 1148–1150.
- [14] a) T. Yildirim, M. R. Hartman, *Phys. Rev. Lett.* **2005**, *95*, 215504–215507; b) H. Wu, W. Zhou, T. Yildirim, *J. Am. Chem. Soc.* **2007**, *129*, 5314–5315.
- [15] V. K. Peterson, Y. Liu, C. M. Brown, C. J. Kepert, *J. Am. Chem. Soc.* **2006**, *128*, 15578–15579.
- [16] D. Frenkel, B. Smit, *Understanding Molecular Simulation: From Algorithms to Applications*, Academic Press, San Diego, **2002**.
- [17] W. Zhou, H. Wu, M. R. Hartman, T. Yildirim, *J. Phys. Chem. C* **2007**, *111*, 16131–16137.
- [18] A. C. Larson, R. B. Von Dreele, General Structure Analysis System, Report LAUR 86–748. Los Alamos National Laboratory, NM, **1994**.
- [19] T. Düren, Y.-S. Bae, R. Q. Snurr, *Chem. Soc. Rev.* **2009**, *38*, 1237–1247.
- [20] Quantum-ESPRESSO, S. Baroni, A. Dal Corso, S. de Gironcoli, P. Giannozzi, C. Cavazzoni, G. Ballabio, S. Scandolo, G. Chiarotti, P. Focher, A. Pasquarello, K. Laasonen, A. Trave, R. Car, N. Marzari, A. Kokalj, <http://www.pwscf.org/>.

Received: October 3, 2009

Revised: January 22, 2010

Published online: March 31, 2010